Focusing versus Defocusing Nonlinearities due to Parametric Wave Mixing

P. Di Trapani,[1] A. Bramati,[1] S. Minardi,[1] W. Chinaglia,[1] C. Conti,[2] S. Trillo,[2,3] J. Kilius,[1,4] and G. Valiulis[4]

[1]*INFM and Department of Chemical, Physical and Mathemetical Sciences, University of Insubria, Via Lucini 3, 22100 Como, Italy*

[2]*Istituto Nazionale di Fisica della Materia, INFM-RM3, Via della Vasca Navale 84, 00146 Roma, Italy*

[3]*Department of Engineering, University of Ferrara, Via Saragat 1, 44100 Ferrara, Italy*

[4]*Department of Quantum Electronics, Vilnius University, Building 3 Sauletekio Avenue 9, 2040, Vilnius, Lithuania*

(Received 9 August 2000; revised manuscript received 12 January 2001; published 16 October 2001)

We show experimentally and theoretically that cascading due to two-wave parametric frequency conversion in quadratic materials acts as an effective focusing or defocusing nonlinearity, depending not only on mismatch, but also on the selected wave, and the dominant type of process (second-harmonic generation or down-conversion). A dramatic asymmetry of beam spreading and threshold lowering for soliton formation against mismatch is the clear experimental signature of this behavior.

DOI: 10.1103/PhysRevLett.87.183902 PACS numbers: 42.65.Tg, 05.45.Yv, 42.65.Pc, 42.70.Qs

Self-trapped (nondiffractive) wave packets or solitons are the most striking manifestation of self-focusing occurring in Kerr media with positive nonlinear index [1]. However, also second-harmonic generation (SHG) with large phase mismatches $\Delta k = 2k_1 - k_2$, results in an effective self-induced Kerr effect for the fundamental harmonic (FH) beam, i.e., an intensity-dependent index change which is of self-focusing type for $\Delta k > 0$ [2,3]. This so-called cascading effect, due to reiterated up- and down-conversions, is a universal $\chi^{(2)}$ phenomenon occurring also via other mixing processes [3,4]. A renewed interest in cascading has motivated the pioneering observation of parametric solitons in SHG [5], which, unlike solitons in true Kerr media, do not undergo catastrophic blowup in 2 + 1 dimensions [6]. The field of $\chi^{(2)}$ trapping was then enriched by observations of spatial locking in optical parametric amplification (OPA, i.e., down-conversion) of quantum noise [7] or finite seed [8], transverse instabilities [9] and temporal effects [10] in SHG, and Bessel-like or vortex beams in SHG and OPA [11,12]. Theoretically, parametric solitons have also stimulated a deep understanding of soliton stability with fallout in the whole area of nonlinear waves [13].

The studies of quadratic wave mixing of confined wave packets have been carried out by taking for granted that large positive Δk results into self-focusing of parametrically generated light. The aim of this Letter is to show experimentally and theoretically that this is not generally true. Vice versa the outcome of the quadratic wave mixing depends critically on the dominant process (SHG vs OPA) through the launching conditions, and also on which beam is considered. Experimentally, we choose solitons as natural candidates to show the diversity existing between SHG and OPA, for which we present compelling evidence for asymmetric lowering of formation threshold. Conversely, to show the different behavior of the two beams we need a significant departure from solitons. A comprehensive classification of the observed focusing/defocusing features is given by means of a novel reduced model.

We have investigated experimentally focusing and soliton formation in SHG and OPA, by means of a laser source delivering 1.5-ps pulses (measured by autocorrelation). SHG is pumped by a beam at $\lambda_0 = 2\pi/k_0 = 1055$ nm, while in OPA a seed at λ_0 is amplified by a SH pump beam at $\lambda_0/2 = 527.5$ nm. A 3-cm-long LBO (lithium triborate) crystal was chosen in spite of its relatively low nonlinear coefficient $d_{\text{eff}} = 0.85$ pm/V ($\chi = k_0\sqrt{2/(c\epsilon_0 n_1^2 n_2)}\, d_{\text{eff}} \simeq 7 \times 10^{-5}$ W$^{-1/2}$ with $n_1 \simeq n_2 = 1.6$), because of (i) low (virtually zero) two-photon absorption at 527.5 nm; (ii) absence of walk-off due to type I temperature-tuned noncritical phase matching. The measured phase matching temperature, corresponding to peak SHG conversion for a wide FH beam was 159 °C. A nearly Gaussian input pump beam with FWHM diameter of 45 μm was focused on the input face of the crystal, and its energy was measured by a calibrated energy meter. The output beam was imaged onto a CCD camera, where the beam profiles and diameters at both FH and SH are measured by means of suitable filters. Under low power operating conditions, we measure a diffracted output FWHM diameter $d \simeq 150$–200 μm.

First, soliton formation is observed at a well-definite pump input energy threshold E_T, above which the beam widths of both harmonics are locked to a fixed value and do not exhibit appreciable changes in response to large variations of input energy (see also Ref. [5]). The threshold measured in SHG is reported in Fig. 1. It decreases abruptly when crossing from the self-defocusing ($\Delta k < 0$) to the self-focusing ($\Delta k > 0$) side. Although in the latter region the threshold depends smoothly on Δk, the output imbalance (FH to SH energy ratio) at threshold increases considerably with Δk, as shown in Fig. 2.

For comparison, we have measured (see Fig. 3) the soliton threshold in OPA with (fixed) 8 nJ FH seed. In this case, the measurements are limited to a smaller range of $|\Delta k|$ by the onset of competing OPA of quantum noise occurring, for high pumping rates, at different signal-idler (spontaneously phase matched) wavelengths.

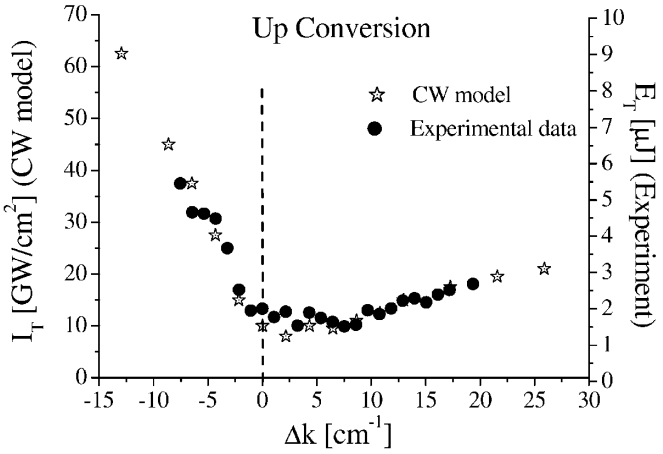

FIG. 1. Threshold energy for soliton formation against mismatch Δk in a SHG experiment. The solid circles are measured data, while stars are relative to the peak intensity calculated numerically from Eqs. (1) within a CW approximation.

Nevertheless, by comparing Figs. 1 and 3, it is clear that OPA shows the opposite trend. The higher threshold measured in OPA for $\Delta k > 0$ suggests that the effective nonlinearity is of defocusing (focusing) type for $\Delta k > 0$ ($\Delta k < 0$), unlike the case of SHG. However, in this case this focusing/defocusing action must be expected to stem from the SH beam which dominates the OPA dynamics.

To check further the focusing versus defocusing nature of the effective nonlinear lensing effect, we have performed a second set of measurements in SHG from an input FH beam with fixed diameter ($d = 44$ μm) and input energy corresponding to the formation of a parametric soliton near phase matching (about 1 μJ, see Fig. 1). Then, the output beam diameters of the FH and SH beams are recorded against mismatch Δk and shown in Fig. 4, in a range of about 100 cm^{-1} corresponding to temperatures 110–200 °C. For large absolute mismatches (say

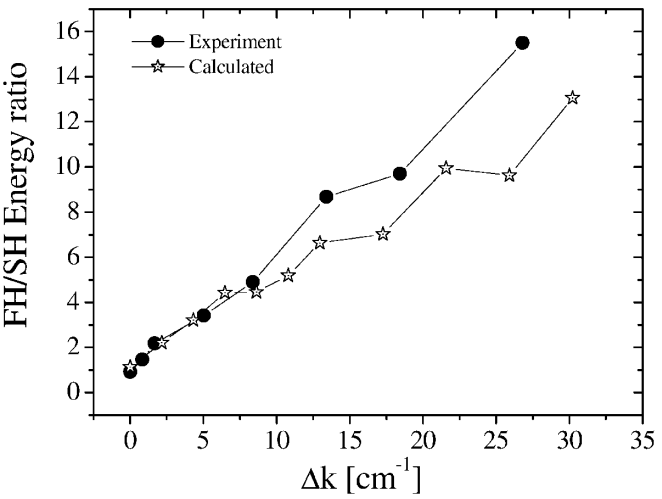

FIG. 2. FH to SH soliton energy ratio versus Δk in SHG.

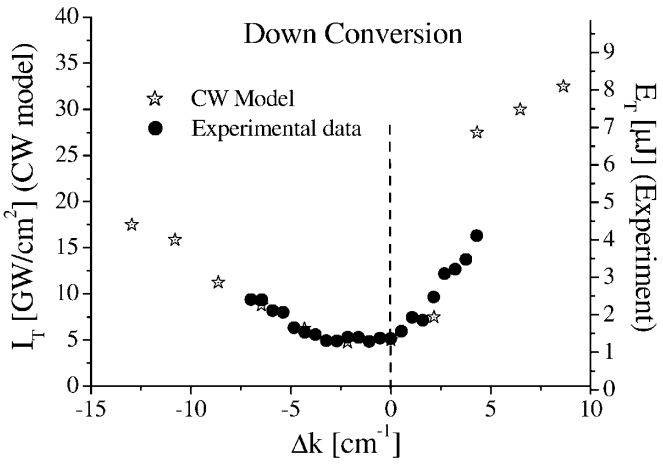

FIG. 3. As in Fig. 1 for an OPA experiment.

$|\Delta k| > 40$ cm^{-1}), diffraction of the FH beam strongly dominates over SHG, and the two beam diameters approach the linear limit, reported as a dashed line in Fig. 4. Here, unlike the previous set of measurements, we do not readjust the input energy to form a soliton when the absolute mismatch is changed. Thus, for intermediate mismatches, the nonlinearity does not balance completely diffraction, and the beams experience significant width variations. Remarkably, the two beams exhibit a strongly asymmetric behavior against reversal of mismatch. For $\Delta k < 0$ the FH beam spreads well above the linear limit following the well-established defocusing nature of the effective nonlinearity. Conversely, for $\Delta k > 0$, it is the SH beam which experiences a significant spread above the linear limit, confirming that the SH beam follows an opposite trend with respect to the FH beam, even in SHG. The data of Fig. 4 are, to the best of our knowledge, the only

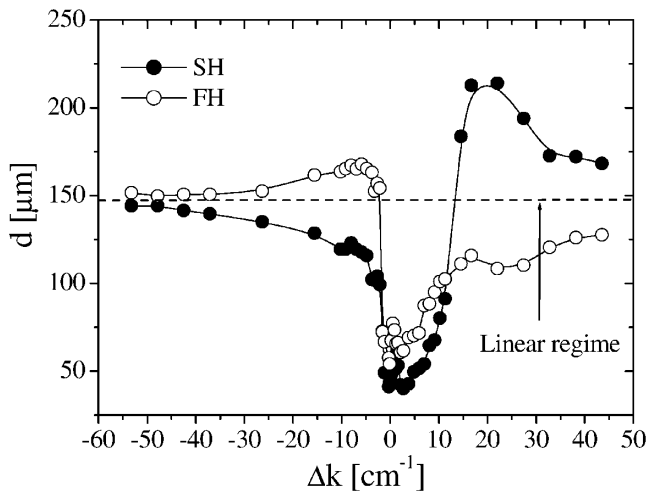

FIG. 4. Output beam FWHM diameters d of the FH and SH beams measured versus mismatch Δk in a SHG experiment with fixed input energy and beam diameter. The dashed line represents the linear limit of diffractive spreading.

compelling evidence that cascading is a subtle limit, with opposite features for the two harmonics.

The observed features can be explained starting from the standard Hamiltonian coupled-mode model [13], conveniently written in terms of dimensionless variables as

$$i\,\frac{\partial u_1}{\partial z} + \frac{\sigma_1}{2}\,\nabla_\perp^2 u_1 + u_2 u_1^* e^{-i\delta k z} = 0\,,$$
$$i\,\frac{\partial u_2}{\partial z} + \frac{\sigma_2}{2}\,\nabla_\perp^2 u_2 + \frac{u_1^2}{2}\,e^{i\delta k z} = 0\,, \tag{1}$$

where $z \equiv Z/Z_d$, $(x,y) \equiv (X,Y)/r_0$ ($r = \sqrt{x^2 + y^2}$ is the radial coordinate, and $\nabla_\perp^2 \equiv \partial_x^2 + \partial_y^2$ the transverse Laplacian), r_0 and $Z_d = k_1 r_0^2$ being a reference input spot-size and diffraction length, respectively. $u_n(x,y,z) = \sqrt{3 - n}\, Z_d \chi E_n(X,Y,Z)$, $n = 1,2$, are slowly varying envelopes, with $|E_n|^2$ being real-world intensities. Here $\delta k \equiv \Delta k Z_d = 2k_0 Z_d(n_1 - n_2)$ is the normalized mismatch, while $\sigma_n \equiv k_1/k_n$, i.e., $\sigma_1 = 1$ and $\sigma_2 \simeq \frac{1}{2}$.

We have dealt with Eqs. (1) following three different approaches, all of them accounting for the observed features. First, we have resorted to numerical integration of Eqs. (1). For any value of Δk, the threshold is determined numerically by doing several simulations at different input intensities. The stars in Figs. 1–3 correspond to the values of threshold and imbalance estimated numerically (the computed threshold is CW and thus reported on a different vertical scale in GW/cm^2). The agreement is satisfactory, although a more quantitative comparison would require accounting for temporal effects (i.e., pulse breaking, group-delay, …), not included in Eqs. (1).

To establish further the asymmetric behavior of mixing, the entire family of radially symmetric nodeless soliton solutions $u_n = u_{n0}(r)\exp(in\beta z)$ of Eqs. (1) [14], was mapped numerically in the plane $(\delta k, \beta)$. Solitons exist for any propagation constant $\beta > 0$ when $\delta k > 0$, and only for $\beta > -\delta k/2$ when $\delta k < 0$, becoming infinitely wide close to this existence threshold. To our purpose, the soliton family is conveniently characterized in terms of power imbalance Q_2/Q_1 (or Q_1/Q_2), where $Q_n = Q_n(\beta, \delta k) = \int\int_{-\infty}^{+\infty} |u_{n0}|^2/(3 - n)\, dx\, dy$ gives the parametric dependence of the FH ($n = 1$) and SH ($n = 2$) powers. Experimentally, one does not have direct control on β, but rather on the (related) total power $Q = Q(\beta, \delta k) = Q_1 + Q_2$ which is conserved along z (together with the Hamiltonian) [13]. The curves showing the dependence of power imbalance Q_2/Q_1 on accessible quantities, i.e., against δk for different constant powers Q, are reported in Fig. 5, and agree with the observed features. First, strongly asymmetric behavior around $\delta k = 0$ is clearly evident. The FH and SH components are comparable only at phase matching, whereas the SH content remains weak for $\delta k > 0$ and is markedly enhanced for $\delta k < 0$ (vice versa for the FH component). Since soliton formation is obviously favored by launching conditions which better match the soliton

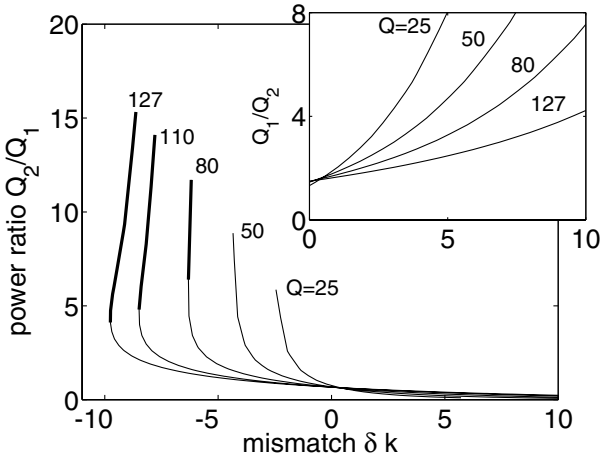

FIG. 5. Ratio Q_2/Q_1 of SH to FH power components versus mismatch δk, for different values of the total soliton power $Q = Q_1 + Q_2$. Unstable soliton branches are plotted as bold curves. The inset shows an enlarged picture of the inverse ratio Q_1/Q_2 for positive δk.

content, this explains why solitons are favored for $\delta k > 0$ in SHG (see Fig. 1), and for $\delta k < 0$ in OPA (see Fig. 3). A second subtle point is the strong asymmetry between the regions of *large* negative and positive mismatches δk. For $\delta k > 0$, Fig. 5 shows that, at constant power, the relative FH content of the soliton raises smoothly (and indefinitely) with δk, in agreement with the quasilinear increase exhibited by SHG data in Fig. 2. Conversely, for $\delta k < 0$, Q_2/Q_1 increases abruptly where, however, solitons become unstable ($dQ/d\beta < 0$ [13], shown as bold branches of the multivalued curves in Fig. 5) thus being unobservable. Despite the instability affects only a tiny region of the plane $(\beta, \delta k)$ close to the existence boundary [13], our accurate calculation shows that solitons exhibit a strong enhancement of SH content exactly within this region. In other words, the parametric soliton instability is the counterpart of the well-known plane-wave decay instability of the SH beam. In this respect, our available data, showing that the SH to FH ratio measured in OPA (not reported) never reaches the high values of SHG imbalance (FH to SH ratio in Fig. 2), support only qualitatively this picture. Conclusive statements on this specific point require overcoming the limitation on the achievable Δk range in OPA, and account for intrinsic Kerr terms.

Last but not least, the essential focusing/defocusing role of cascading nolinearities can be captured from a multiscale reduction [15] of Eqs. (1), taking $\varepsilon = \delta k^{-1}$ as smallness parameter. To this end, the two interacting fields, assumed to depend on both the fast longitudinal scale $\zeta = z/\varepsilon$, and slow scales $z_n = \varepsilon^n z$, $x_n = \varepsilon^n x$, $y_n = \varepsilon^n y$, $(n = 0, 1, 2, \ldots)$, are expanded as $u_1 = A + \varepsilon A_1 + \varepsilon^2 A_2 + \ldots$, and $u_2 = B + \varepsilon B_1 + \varepsilon^2 B_2 + \ldots$, without any assumption on their relative magnitude. By proceeding in a standard way [15] (details will be published elsewhere), we obtain in terms of original variables, the

reduced system obeyed by the leading-order envelopes A and B as

$$i\frac{\partial A}{\partial z} + \frac{1}{2}\nabla_\perp^2 A + \frac{1}{2\delta k}|A|^2 A - \frac{1}{\delta k}|B|^2 A = 0,$$
$$i\frac{\partial B}{\partial z} + \frac{\sigma_2}{2}\nabla_\perp^2 B - \frac{1}{\delta k}|A|^2 B = 0. \quad (2)$$

Although Eqs. (2) do not account for the parametric energy conversion since they conserve the individual beam powers, they describe correctly the large-scale dynamics (averaged over many periods of conversion and back-conversion) for large $|\delta k|$, thus generalizing the self-consistent nonlinear Schrödinger equation (NLSE) description of cascading. As compared with previous multiscale derivations [16], self-action at SH does not appear, since it involves coupling to higher harmonics for which no experimental evidence was ever reported. The form of the effective cubic terms in Eqs. (2) is similar to those found for quasi-phase-matching gratings [17] (where, however, they act as a correction to grating-induced phase-matched quadratic terms), thus suggesting their universal role for parametric mixing of mismatched waves. Importantly, the global lensing effect arising from phase curvature in Eqs. (2) is affected by both self-induced (at FH) and cross-induced terms which compete and act oppositely for a fixed δk. This explains the observed physics at a glance. First, in SHG ($|A| \gg |B|$) the two harmonics experience defocusing action for opposite signs of δk, in agreement with the data reported in Fig. 4. Second, lower threshold is expected where the effective nonlinearity dictated by the dominant beam, i.e., FH in SHG and SH in OPA ($|B| \gg |A|$), has self-focusing nature thereby balancing diffraction. According to Eqs. (2), in agreement with Figs. 1 and 3, this occurs for $\delta k > 0$ in SHG, and for $\delta k < 0$ in OPA, respectively. In the focusing regions of SHG and OPA, the inverse dependence of the effective Kerr coefficients on δk in Eqs. (2) accounts for the slight increase of threshold with mismatch. More importantly, Eqs. (2) in combination with Fig. 5 shows physically that solitons are allowed to exist for $\delta k < 0$ because the dominant SH component experiences a self-focusing action. In other words, contrary to common belief, both signs of δk must be regarded as self-focusing as long as the prevailing soliton component is considered.

Finally, note that our reduced model is consistent with the well-known NLSE limit, which is obtained from Eqs. (2) with $B = 0$. In this case, an axially symmetric self-trapped FH beam $u_1 = A(r)$ is accompanied by a stabilizing SH field which, in our approach arise at order ε as $u_2 = \varepsilon B_1 = (A^2/2\delta k)\exp(i\delta k z)$. These soliton solutions approximate the exact ones of Fig. 5 only for $\delta k \gg 1$. Importantly, in OPA a singular self-consistent equation for a single beam amplitude cannot be derived, even for large Δk. This is due to the fact that the FH beam is weak, and the beam dynamics remains determined by the cross-induced origin of nonlinear phase curvature in Eqs. (2).

In summary, the concept of self-focusing (defocusing) originating from parametric conversion depends not only on the mismatch sign, but also upon the selected wave and the dominant process (SHG or OPA). The physics of this phenomenon is inherently contained in the usual coupled-mode model for two-wave mixing. Striking asymmetries between soliton thresholds and evolutions of nonsoliton beam diameters confirm this picture.

This work was funded by INFM (PAIS Project 1999) and Project Unesco Uvo-Roste 875.571.0.

[1] R. Y. Chiao, E. Garmire, and C. H. Townes, Phys. Rev. Lett. **13**, 479 (1964).
[2] L. A. Ostroskii, Sov. Phys. JETP **24**, 797 (1967).
[3] G. I. Stegeman, D. J. Hagan, and L. Torner, Opt. Quantum Electron. **28**, 1691 (1996).
[4] Ch. Bosshard *et al.,* Phys. Rev. Lett. **74**, 2816 (1995).
[5] W. E. Torruellas *et al.,* Phys. Rev. Lett. **74**, 5036 (1995); R. Schiek, Y. Baek, and G. I. Stegeman, Phys. Rev. E **53**, 1138 (1996). These experiments were carried out only recently in spite of an early prediction by Y. N. Karamzin and A. P. Sukhorukov, JETP Lett. **20**, 338 (1975).
[6] L. Bergé, Phys. Rep. **303**, 259 (1998), and references therein.
[7] P. Di Trapani *et al.,* Phys. Rev. Lett. **80**, 265 (1998).
[8] M. T. G. Canva *et al.,* Opt. Lett. **22**, 1683 (1997); R. A. Fuerst *et al.,* Opt. Quantum Electron. **30**, 907 (1998).
[9] R. A. Fuerst *et al.,* Phys. Rev. Lett. **78**, 2756 (1997).
[10] P. Di Trapani *et al.,* Phys. Rev. Lett. **81**, 570 (1998); X. Liu, L. J. Qian, and F. W. Wise, Phys. Rev. Lett. **82**, 4631 (1999); X. Liu, K. Beckwitt, and F. W. Wise, Phys. Rev. E **61**, R4722 (2000).
[11] P. Di Trapani *et al.,* Phys. Rev. Lett. **81**, 5133 (1998); T. Wulle and S. Herminghaus, Phys. Rev. Lett. **70**, 1401 (1993).
[12] P. Di Trapani *et al.,* Phys. Rev. Lett. **84**, 3843 (2000).
[13] D. E. Pelinovsky, A. V. Buryak, and Yu. S. Kivshar, Phys. Rev. Lett. **75**, 591 (1995); A. V. Buryak, Yu. S. Kivshar, and S. Trillo, Phys. Rev. Lett. **77**, 5210 (1996).
[14] L. Torner, Opt. Commun. **114**, 136 (1995); A. V. Buryak, Yu. S. Kivshar, and V. V. Steblina, Phys. Rev. A **52**, 1670 (1996).
[15] A. H. Nayfeh, *Introduction to Perturbation Techniques* (Wiley, New York, 1993).
[16] A. G. Kaloksai and J. W. Haus, Phys. Rev. A **49**, 574 (1994); Phys. Rev. E **52**, 1636 (1995).
[17] C. B. Clausen, O. Bang, and Y. S. Kivshar, Phys. Rev. Lett. **78**, 4749 (1997).